Biosensors and Bioelectronics 245 (2024) 115836

Contents lists available at ScienceDirect

Biosensors and Bioelectronics

journal homepage: www.elsevier.com/locate/bios

SERS-based pH-Dependent detection of sulfites in wine by hydrogel nanocomposites

Deniz Yilmaz [a,1], Bruno Miranda [b,1], Enza Lonardo [c], Ilaria Rea [b], Luca De Stefano [b,*], Anna Chiara De Luca [a,**]

[a] Institute for Experimental Endocrinology and Oncology, "G. Salvatore" (IEOS), National Research Council of Italy (CNR), Naples, Italy
[b] Institute of Applied Sciences and Intelligent Systems (ISASI), National Research Council of Italy (CNR), Naples, Italy
[c] Institute of Genetics and Biophysics (IGB), National Research Council of Italy (CNR), Naples, Italy

ARTICLE INFO

Keywords:
Sulfites/SO_2
Wine
SERS
Hydrogel
AuNPs
Optical sensing

ABSTRACT

Sulfur dioxide (SO_2) and sulfites are well-known additives in winemaking due to their preservative properties. Although they can prevent oxidation and inhibit microbial growth, they pose health risks and require limitations on their use. Consequently, the total level of SO_2 is regulated and several quantification strategies have been proposed. The approved detection methods require the extraction of SO_2 by heating and/or acid treatment. Then, iodine or acid/base titrations are conducted for the detection of liberated SO_2. Although these methods can provide sensitive detection of SO_2, they are complex, time-consuming, and require sample preparation steps and skilled operators. Thus, to overcome these disadvantages, an easy-to-use method, involving simple sample preparation steps, and offering high sensitivity and selectivity, is desirable. Herein, we introduce a SERS-based strategy for SO_2 detection in liquids using hydrogel nanocomposites. The hydrogels are prepared by poly (ethylene glycol) diacrylate (PEGDA) in the presence of gold nanoparticles (AuNPs), acting as the SERS substrate. The use of hydrogels ensures a homogenous signal distribution and an efficient collection of SO_2, and drying the hydrogels enhances and stabilizes the obtained SO_2 signal. The detection strategy is based on the pH-dependent dissociation of SO_2. By adjusting the pH value of wine to 10 through simple dilutions, SO_2 can be directly detected in wine, down to 0.4 ppm, well below the regulatory limits. The proposed method allows for sensitive, direct, cost-effective detection of SO_2 by eliminating the loss of the gaseous form of the sample and avoids titration-based detection methods.

1. Introduction

Sulfur dioxide (SO_2) and sulfites are widely used in many different foods and beverages, especially in wine for their antioxidant and antimicrobial properties (Gómez-Plaza and Bautista-Ortín, 2019; Guerrero and Cantos-Villar, 2015; Ozbek and Akman, 2013). They provide a redox reaction with oxygen, which prevents the oxidation of other compounds. Moreover, they can also prevent wine browning, color loss during wine aging, and it can help wine maintain its flavor and freshness (Grogan, 2015; Santos et al., 2012). Despite all advantages, SO_2 can cause allergic reactions which can lead to respiratory and cardiovascular diseases, including asthma, lung cancer, and respiratory infections (Lee et al., 2002; Timbo et al., 2004; Vally et al., 2009; Vally and Thompson, 2001). Moreover, it is also known that sulfite derivatives can cause proto-oncogenes activation, tumor suppressor gene inactivation, and even pathogenesis of SO_2-associated lung cancer (Qin and Meng, 2009). Thus, the levels of SO_2 need to be monitored, and legal limits are regulated at 150–200 ppm in wines (Stockley et al., 2021). Internationally recognized methods for SO_2 detection are titration-based analytical methods, where SO_2 is first extracted from the wine samples by heating and acidifying and then analyzed by iodine or acid/base titration (OIV-MA-AS323-04A, OIV-MA-AS323-04B). However, these methods are labor-intensive, time-consuming, require complex sample preparation steps, and have limited accuracy and sensitivity. Moreover, it is also known that pre-processing of the wine samples disrupts the SO_2 equilibrium and thus causes an overestimation of the SO_2 amount in the

* Corresponding author.
** Corresponding author.
E-mail addresses: luca.destefano@cnr.it (L. De Stefano), annachiara.deluca@cnr.it (A.C. De Luca).
[1] These authors contributed equally.

https://doi.org/10.1016/j.bios.2023.115836
Received 8 September 2023; Received in revised form 18 October 2023; Accepted 9 November 2023
Available online 17 November 2023

sample. They are also highly affected by the matrix and have repeatability problems which causes limited sensitivity and accuracy (Coelho et al., 2015; Howe et al., 2018). On the other hand, several other methods have been recently proposed, including high-performance liquid chromatography (HPLC), liquid chromatography-mass spectrometry (LC-MS), and gas chromatography-mass spectrometry (GC-MS) (Koch et al., 2010; Monro et al., 2012; Oliveira et al., 2009; Theisen et al., 2010). Even though these methods solve the sensitivity and accuracy problems for detection, they require complicated sample preparation steps, skilled operators, and a long time for detection. Therefore, there is still a significant demand for the development of point-of-need devices that can perform fast and sensitive analysis in situ, by non-specialized personnel.

In this context, surface-enhanced Raman scattering (SERS)-based protocols have been proposed for the detection of pesticides and additives in foods and beverages (Paschoalin et al., 2022; Xing et al., 2022). Specifically, SERS-based SO_2 detection strategies for wine are summarized in Table 1. The first was based on a thin-film microextraction process providing SO_2 detection down to 0.1 ppm (0.8 μM) (Deng et al., 2015). Another group proposed an extraction protocol on a microfluidic paper-based analytical device for capturing SO_2. The conversion of 4-mercapto-pyridine to methyl sulfate yielded a limit of detection (LOD) of 1 μM (Li et al., 2018). Kong et al. employed a headspace sampling strategy to detect SO_2 in wine with 1 μM LOD using N, N-Bis (2-hydroxyethyl) ethylenediamine (HEEDA) as the recognition element and a silver nanofilm as the SERS substrate (Kong et al., 2021). In a different approach, metal-organic framework hybrid films were proposed for SO_2 detection achieving an LOD of 1 μM (Huo et al., 2022). Mandrile et al. adopted a different approach by employing solid-phase extraction to remove interfering compounds in wine. They directly detected SO_2 in the cleaned wine samples by adding AgNPs and achieved LOD down to 0.6 ppm (0.5 μM) (Mandrile et al., 2020).

As observed, most of these traditional and novel protocols use headspace sampling for the extraction of SO_2, allowing for the discrimination of volatile compounds from interfering nonvolatile ones, but requiring long and complicated pre-processing of wine samples with excess amounts of acid and heat. These steps lead to sample loss and limit the sensitivity (Ross, 2012).

Direct measurement from wine samples could offer advantages in terms of simplicity, sensitivity, and elimination of gaseous compounds' loss. In this context, nanocomposite transducers made of hydrogels and plasmonic nanoparticles (NPs) are emerging as promising alternatives to conventional optical biosensors (Theisen et al., 2010; Miranda et al., 2021a; Pastoriza-Santos et al., 2018). Specifically, SERS-based plasmonic/hydrogel nanocomposites can harness the formation of dynamic hotspots, in which the swelling of the hydrogel allows for the entrapment of the targets, while its shrinkage enables the increase in hotspot density (Aldeanueva-Potel et al., 2009; Fateixa et al., 2014; Miranda et al., 2021b).

In this study, we developed a SERS substrate based on poly(ethylene glycol) diacrylate (PEGDA)/Gold Nanoparticles (AuNPs) hydrogel nanocomposites for the direct detection of SO_2 from liquid samples. AuNPs were used as the plasmonic nanomaterial for SERS-based detection, while hydrogels as the flexible support that facilitated a homogenous signal distribution by entrapping the volatile molecules and enhancing the SO_2 signal upon drying. For the direct detection of SO_2 from wine samples, we used the pH-dependent dissociation of SO_2. The proposed system exhibited a linear detection range of 0.1–10 ppm, with a LOD of about 0.4 ppm (3.2 μM). The comparison with the official method provided consistent results, demonstrating that it could be an effective point-of-need device for fast, cost-effective, and easy on-site applications with high selectivity and sensitivity.

2. Results & discussion

2.1. SERS nanocomposites fabrication and characterization

For the detection of sulfur dioxide in wine, a flexible nanocomposite substrate is designed. Flexibility arises from PEGDA, which can trap small volatile molecules and also provide a highly homogeneous signal distribution. High molecular weight PEGDA was chosen for its great swelling capacity in contact with liquids, as well as its high thermal stability. Moreover, PEGDA shows excellent transparency, enabling the detection of signals originating from the embedded optical nanomaterials (Cavallo et al., 2017; Miranda et al., 2022).

The optical transducing nanomaterial consists of AuNPs, which significantly enhance the Raman signal of the target molecules. Their standardized, simple, and large-scale fabrication strategies together with high chemical stability, and SERS activity enable the detection of small molecules (Managò et al., 2021; Nocerino et al., 2022; Spaziani et al., 2023). Furthermore, their known interaction with sulfur-containing molecules (Nuzzo and Allara, 1983; Xue et al., 2014) was expected to provide interaction with target SO_2 and thus enhance sensitivity.

The AuNPs were fabricated *via* the seeded-growth method as reported by Bastus et al. in different sizes (Bastús et al., 2011) (Section 1.2 of SI). The details on synthesis and characterization as well as the selection of the best-performing AuNPs size are reported in sections 3.1

Table 1
Reported SERS-based SO_2 detection strategies from wine. Linear range and LOD values are converted into micromolar levels for label-free approaches using the main SO_2 source in each study.

	Extraction Method	SERS Substrate	Matrix	Recognition Element	Linear Range	LOD	Ref
Labeled Approach	Headspace extraction	AuNRs	PAD	MPY	1–2000 μM	1 μM	Li et al. (2018)
	Headspace extraction	Ag nanofilm	–	HEEDA	1–10^4 μM	1 μM	Kong et al. (2021)
	Headspace extraction	AgNPs	MOF	TM	10^{-2} – 10^3 μM	1 μM	Huo et al. (2022)
Label-free Approach	Headspace extraction	AuNPs	ZnO substrate	–	1–200 ppm (8–1600 μM)	0.1 ppm (0.8 μM)	Deng et al. (2015)
	Solid phase extraction	AuNPs	Gas Diffusion PAD	–	5–300 ppm (40–2400 μM)	2 ppm (16 μM)	Chen et al. (2016)
	Solid phase extraction	AgNPs	–	–	0–100 ppm (0–800 μM)	0.6 ppm (4.8 μM)	Mandrile et al. (2020)
	No extraction	AuNPs	PEGDA Hydrogel	–	0.1–10 ppm (0.8–80 μM)	0.4 ppm (3.2 μM)	This work

Abbreviations: AuNRs, gold nanorods; AuNPs, gold nanoparticles; AgNPs, silver nanoparticles; AgNCs, silver nanocubes; PAD, paper-based analytical device; MOF, metal-organic framework; ZnO; zinc oxide, MPY; 4-mercaptopyrinde; HEEDA, N,N-Bis (2-hydroxyethyl) ethylenediamine; TM, thiol magenta; APDS, 4-aminophenyl disulfide.

and 3.2 of SI (see also Fig. S1, Table S1, Fig. S2). 60 nm AuNPs were selected as the best-performing AuNPs size due to the highest signal intensity and thus highest sensitivity. For the hydrogel nanocomposite fabrication, 60 nm AuNPs were concentrated up to a final AuNPs/PEGDA concentration of 10% w/w, suspended in a PEGDA pre-polymer solution containing the photoinitiator, and crosslinked under UV light (Fig. 1a and section 1.3 of SI).

The mean absorbance spectra of 60 nm AuNPs in solution and within the hydrogel are shown in Fig. 1b and c. The plasmonic resonance of the AuNPs is centered at ~540 nm, while a second band together with a redshift of the resonance is observed after embedding them in the hydrogel. SERS performance of the hydrogel nanocomposites was characterized with biphenyl-4-thiol (BPT) (Verde et al., 2021). For SERS measurements, three independent measurements were obtained. In each measurement, 5 SERS maps with 100 acquisitions from different regions of hydrogel were acquired (Scheme S2). A total of 1500 acquisitions is averaged and used for comparison with other groups. Detailed information is given in Section 1.7 of SI.

An excellent signal intensity (Fig. 1d), and an enhancement factor (EF) about 0.9×10^6 with good spectral reproducibility (within 10%) (Fig. 1e) were achieved. Differently from the self-assembling or drop-casting of AuNPs in/on a polymeric network, the adopted all-solution fabrication strategy provides uniform distribution of the AuNPs within the hydrogel, enhanced stability, tunable optical properties (Miranda et al., 2021b), with subsequent highly uniform SERS signal intensity distribution.

The proposed device resulted as highly stable to temperature, pH, and ionic strength treatments as reported in section 3.3 of SI (Fig. S3).

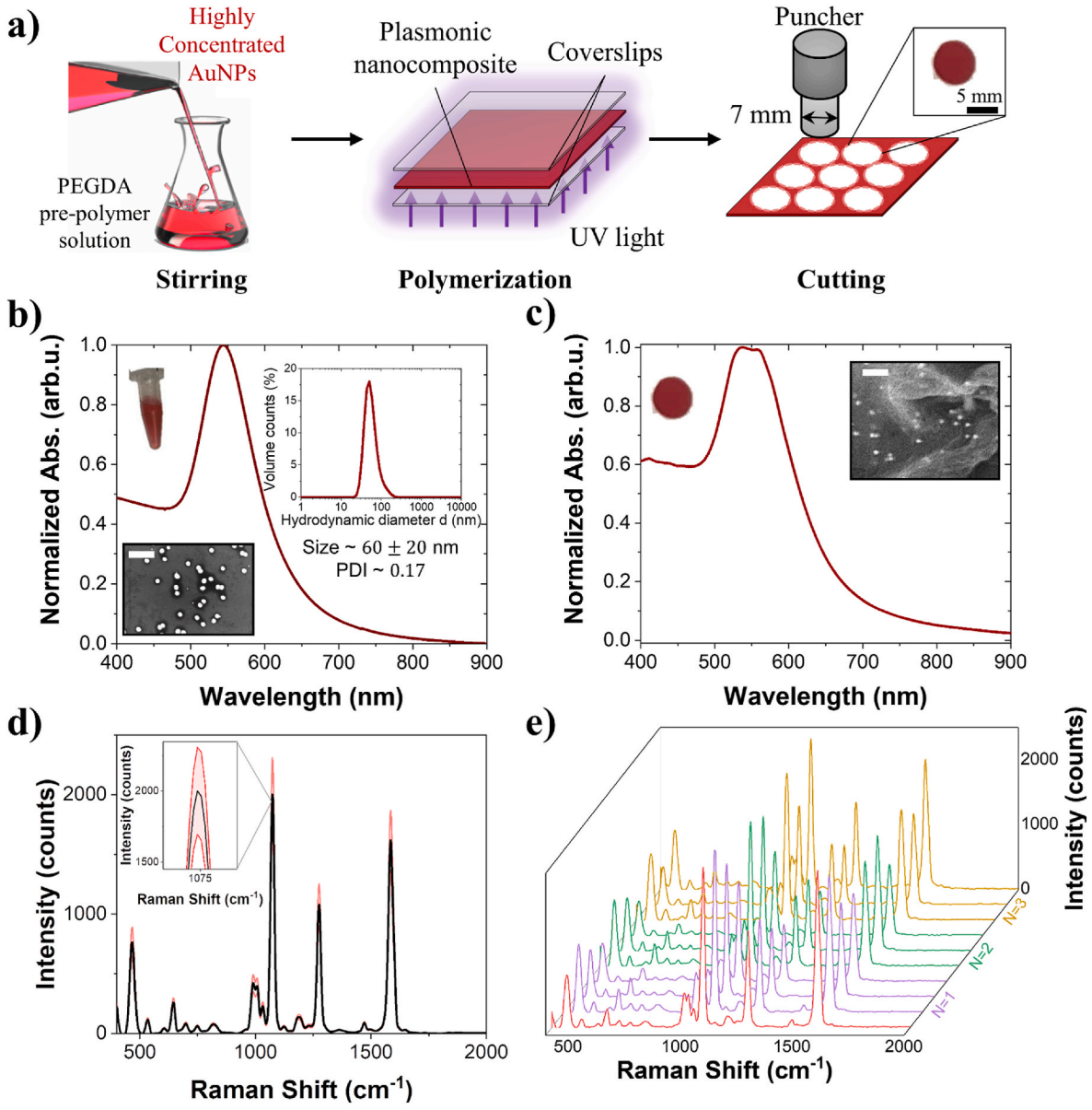

Fig. 1. a) Schematic representation of the fabrication strategy of PEGDA AuNPs nanocomposites, b) Normalized mean absorbance spectra of 60 nm AuNPs in solution. In the inset (bottom left), SEM image of AuNPs dried on a silicon wafer. The scale bar is 500 nm. In the inset (top right), the hydrodynamic size distribution of AuNPs in solution. c) Normalized mean absorbance spectra of 60 nm AuNPs in the hydrogel. In the inset, SEM images of nanocomposites in the swollen state. The scale bar is 500 nm. d) Average SERS spectrum of 60 nm AuNPs in hydrogel incubated with 1 mM BPT, reported as mean ± SD from three independent measurements. Inset: Zoom in to the BPT peak at 1075 cm^{-1}. e) Variability of BPT (1 mM) SERS signals on hydrogels from three independent measurements with three acquisitions in each. Each independent measurement is reported by different colors. The mean spectrum is shown in red.

2.2. Detection performance of hydrogel nanocomposites

After selecting the best AuNPs size (see sections 3.1 and 3.2 of SI), the performance of the hydrogel nanocomposites was investigated both in wet and dry conditions to increase the number of available hotspots (see sections 1.4 and 3.1 of the SI for experimental details). Representative images of both conditions are reported in Fig. 2a–d. As seen, large pores are present in the swollen state (Fig. 2a,c). The AuNPs are well dispersed within the material and far apart to be considered as poorly interacting. Vice versa, in shrunk hydrogels, the large pores collapse among them due to the water evaporation (Fig. 2b,d). The AuNPs are still dispersed within the hydrogel, but there is the formation of a greater number of clusters. It must be noted that only the superficial layer of the hydrogel could be observed by SEM imaging, and that, soon after the first layer, other AuNPs are readily available to form other clusters.

COMSOL Multiphysics software was used to perform numerical simulations of the field distribution. A 1 μm × 1 μm area was randomly selected from Fig. 2c–d to define the geometry (Figs. S4a–b) and derive the theoretical field enhancement (FE) for both swollen and shrunk states (Fig. 2e–f, respectively) (see section 1.10 of SI). In the first case, the AuNPs available in the region of interest were considered immersed in a medium with an effective refractive index of 1.34, considering that high MW PEGDA is mainly composed of water (Fig. S4c). In this case, the maximum computed FE was 4. In the second case, due to the collapsing of PEGDA during water evaporation, AuNPs were considered immersed in a medium only made of polymerized PEGDA, having a refractive index of 1.51 (Fig. S4c). In this case, the maximum FE resulted as 20 because of the formation of hotspots between two AuNPs. Therefore, a 5-fold increase of the FE was numerically estimated by introducing the drying step. To verify numerical simulations, BPT was let to diffuse within the hydrogel network and interact with AuNPs. SERS measurements were performed in wet and dried hydrogel nanocomposites (Fig. 2g and h, respectively). In both conditions, good spectral variability (Fig. 1e and Fig. S5) was achieved. Drying the hydrogels provided a 5-fold increase in the BPT SERS intensity with a subsequent increase of the EF from 0.9×10^6 to 5×10^6 in excellent agreement with the numerical simulations. The EF increase can be explained by the formation of a higher number of hotspots among plasmonic NPs in the dried state; indeed, AuNPs within the hydrogel network come in close proximity when the excess water is removed from the hydrogel (*dynamic hotspots*) (Abalde-Cela et al., 2011; Aldeanueva-Potel et al., 2009; Miranda et al., 2022). Moreover, the effective refractive index of the medium in the surroundings of the AuNPs undergoes a significant increase from the wet to the dried states, thus causing an increase in the decay length of the plasmonic resonance (Maier, 2007).

While BPT is a standard molecule capable of interacting with AuNPs and forming a monolayer on AuNPs, this work aimed to achieve the quantitative detection of sulfites in a real matrix, such as wine. The reason for .the selection of a plasmonic flexible nanocomposite substrate was to trap desired small volatile molecules and enhance their Raman signal. AuNPs are used not only for the enhancing Raman signal from target molecules but also due to the affinity of the sulfur-containing molecules to the AuNPs. These are key elements for the detection of SO_2 in wine, as SO_2 is a volatile component, which generally requires volatilization steps and gaseous phase detection protocols. Indeed, we designed our system to trap the volatile SO_2 molecule directly from the liquid samples without using any volatilization procedure and headspace sampling. Thus, to understand the performance of the designed

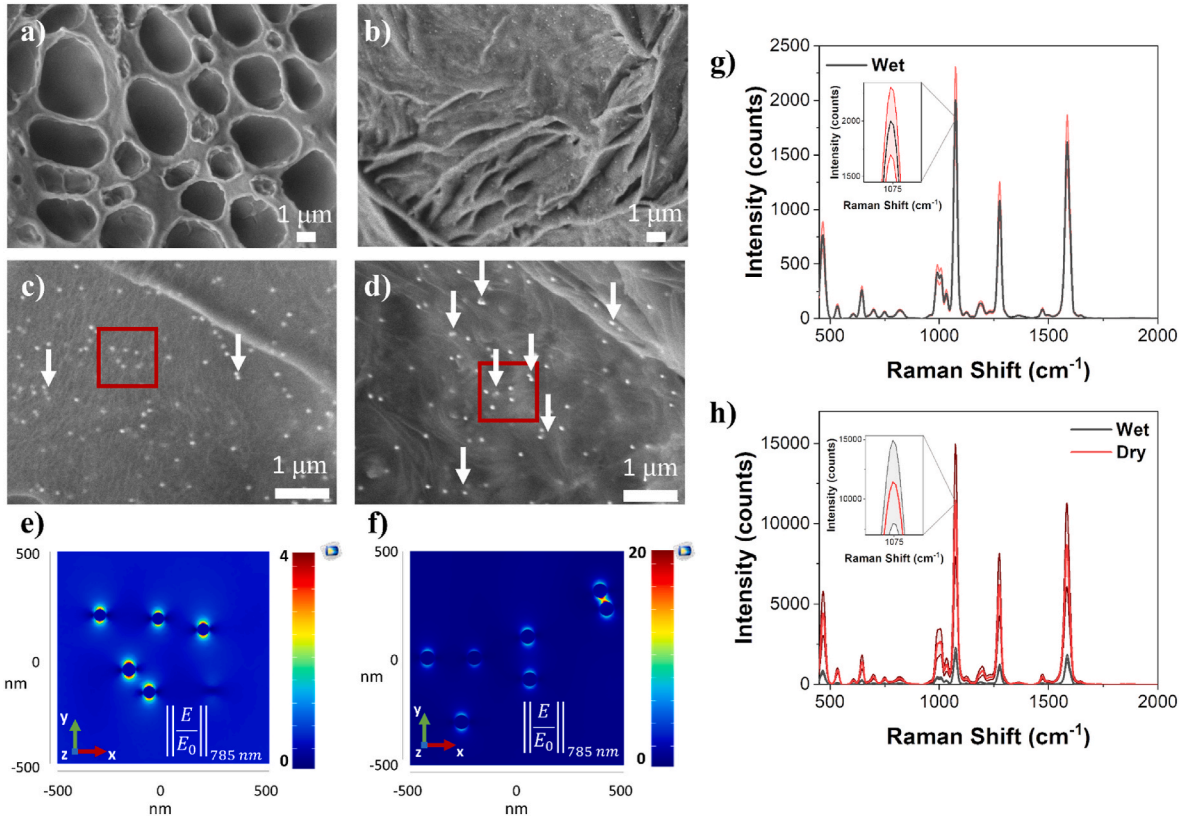

Fig. 2. Low magnification SEM images (7000×) of hydrogel nanocomposites a) in the wet state and b) in the dry state. High magnification SEM images (12000×) of hydrogel nanocomposites c) in the wet state and d) in the dry state. The red squares denote the 1 μm × 1 μm area used for numerical simulations. White arrows show the presence of small clusters of AuNPs. e) 2D plot of the norm of the electric field (normalized to the background field) on a plane centered at the center of 60 nm AuNPs obtained for AuNPs immersed in a material with e) an effective refractive index of 1.34 (wet hydrogel and f) an effective refractive index of 1.51 (dry hydrogel). The average SERS spectrum of 60 nm AuNPs hydrogel incubated with 1 mM BPT g) in wet and h) compared with dried conditions, reported as mean ± SD from three independent measurements Insets: Zoom in to the BPT peak at 1075 cm^{-1}.

system for the detection of volatile SO_2, the obtained signals from SO_2 in hydrogels were compared with drop-cast 60 nm AuNPs on glass both in wet and dried (see section 1.4 in the SI) conditions as shown in Fig. 3. For all measurements, $K_2S_2O_5$ was used as the source of SO_2, which forms SO_2 in solution with the reaction in **eq. S1** (Stockley et al., 2021) (see section 2 of SI). In all cases, characteristic peaks of SO_2 were observed at 625 cm^{-1} attributed to O–S–O symmetric bending and 928 cm^{-1} attributed to S–O symmetric, asymmetric stretching (Chen et al., 2016; Huo et al., 2022; Mandrile et al., 2020).

The drop-cast 60 nm AuNPs both in the wet (Fig. 3a), and dry (Fig. 3b) conditions provided low reproducibility in measurements due to the uncontrolled distribution of AuNPs when they were dried on a surface. Moreover, when they were compared, no significant spectral differences were observed. Indeed, the peak intensity at 625 cm^{-1} of SO_2 was found as similar in both states, which means that the interaction of SO_2 with AuNPs in the absence of the hydrogel is not affected by the drying process.

Differently, in the case of hydrogels, wet (Fig. 3c), and dry (Fig. 3d) conditions were significantly different. The same concentration of SO_2 (400 ppm) exhibited a poor SERS intensity (<50 counts) for wet hydrogels, while it reached an extremely high SERS intensity after their drying (~10^4 counts). The very different behavior between wet and dry hydrogels is only partly justified by the increased number of hotspots and higher refractive index of the substrate after shrinkage, as shown in Fig. 2 for BPT molecules. However, an explanation can be found starting from the chemical nature of sulfites as well. SO_2 in its molecular form is highly volatile, but when in solution it tends to diffuse within the hydrogel network. We speculate that, during the drying process, once the shrinkage of the network occurs, sulfite molecules remain entrapped within the network in the surroundings of AuNPs. A uniform and stable signal over time is achieved, in such a way that its SERS signal can be measured with high sensitivity as well as accuracy.

2.3. Optimization of pH measurement conditions

The best-performing hydrogel nanocomposites were tested with $K_2S_2O_5$ solutions at different concentrations in water, as the first trial (Fig. S6a). As seen, the SO_2 signal suddenly drops down at concentrations lower than 400 ppm due to the instability of the solution and the pH-dependent dissociation of SO_2. Indeed, in an aqueous solution, SO_2 is present in three different pH-dependent forms such as molecular SO_2, HSO_3^- (bisulfite), and SO_3^{2-} (sulfite). At wine pH (~3), there are both molecular SO_2 and bisulfite forms (**eq. S2**) and the dominant form is bisulfite. Starting from pH 5, sulfite starts to form, and, at pH 8 (**eq. S3**), the dominant version switches from bisulfite to sulfite (Cojocaru and Antoce, 2012; Corte et al., 2012). To understand this behavior, citric acid buffer at pH 3 was introduced (Fig. S6b). Even though citric acid buffer solves the stability problem, no signal from molecular SO_2 and HSO_3^- was detected.

Thus, to understand if the system was capable of detecting sulfite form instead of bisulfite and molecular SO_2 forms, pH was increased gradually up to 10. In the first place, the experimental design was constructed based on the use of different buffers for each pH (acetate buffer for pH 5, potassium phosphate buffer for pH 8, and carbonate buffer for pH 10). However, due to the well-known effects of buffer conditions on SERS measurements (Israelsen et al., 2015), each buffer was also forced to all the other pH values to eliminate any interference. When the signal coming from the buffers was checked (control spectrum in each graph as CTRL), no interferences were observed (Fig. 4).

When the pH-dependent change of the signal was evaluated, higher signal intensity was achieved at higher pH values (Fig. 4a–c). Indeed, as mentioned above, at pH 3, bisulfite and molecular SO_2 are present, and the dominant form is bisulfite. After pH 5, sulfite starts to form and the amount of bisulfite decreases with increasing pH (Corte et al., 2012). Thus, at pH 3, almost no signal was observed because bisulfite and molecular SO_2 forms were not suitable to diffuse within the proposed hydrogel nanocomposite. However, starting from pH 5, signal intensities increased due to the formation of sulfite. Then, the highest signal was

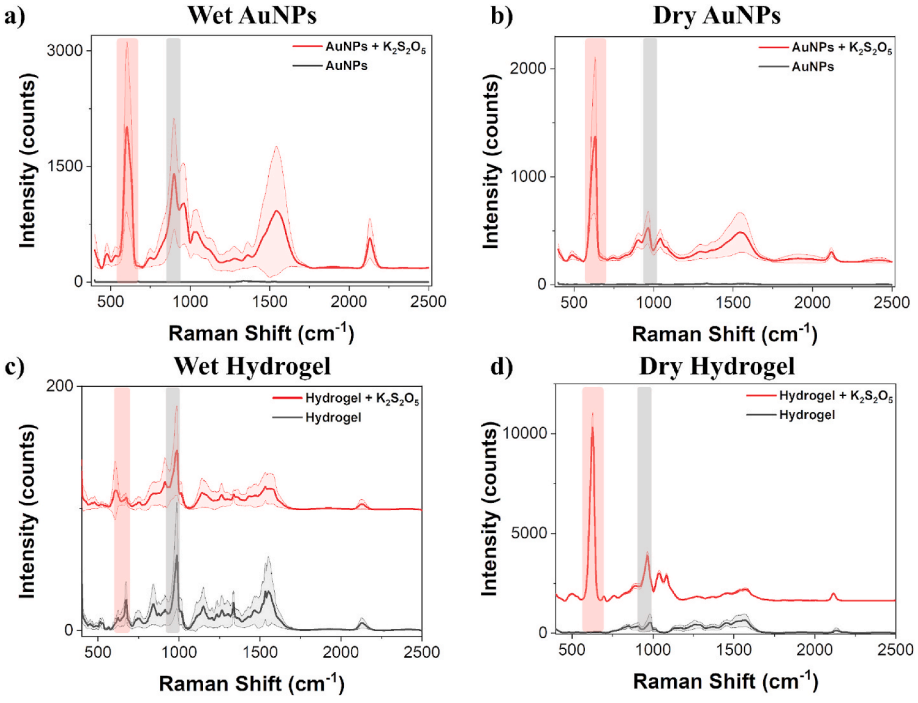

Fig. 3. SERS spectrum of a) $K_2S_2O_5$ solution on drop-cast AuNPs, b) $K_2S_2O_5$ solution dried on drop-cast AuNPs, c) $K_2S_2O_5$ solution in hydrogel nanocomposites, and d) $K_2S_2O_5$ solution dried with hydrogel nanocomposites. $K_2S_2O_5$ concentration is kept constant at 400 ppm. In each spectrum SO_2 characteristic peak of 625 cm^{-1} is highlighted in red and 928 cm^{-1} in grey. Each spectrum is compared with the relative background without any further treatment and reported as mean ± SD from three independent measurements. Spectra are horizontally shifted for visual clarity.

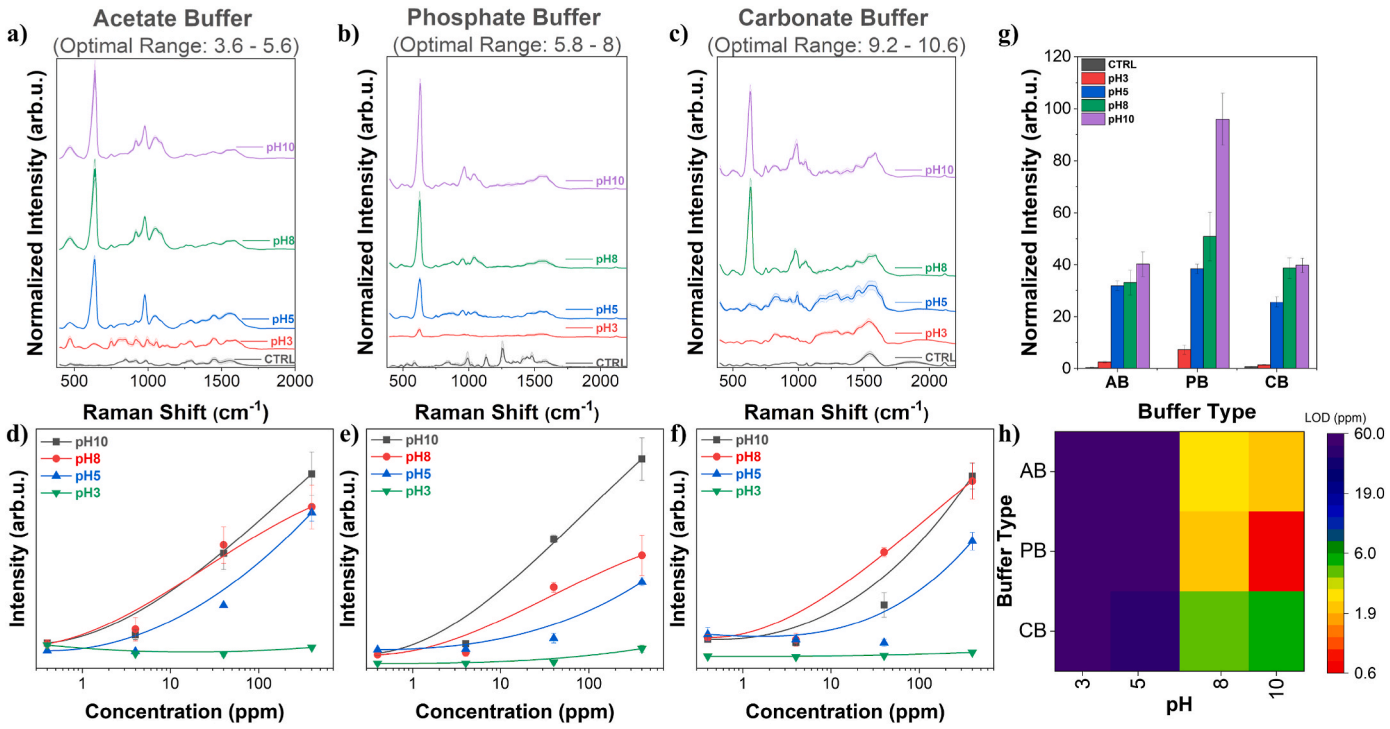

Fig. 4. Evaluation of pH-dependent behavior of SO_2 within dried hydrogels. SERS spectrum of dried hydrogel nanocomposites in a, d) acetate buffer (AB), b, e) potassium phosphate buffer (PB), and c, f) carbonate buffer (CB). CTRL groups are relevant buffers incubated within dried hydrogels in the absence of $K_2S_2O_5$. a-c) 400 ppm $K_2S_2O_5$ and d-f) SERS signal intensity at 625 cm^{-1} as a function of $K_2S_2O_5$ concentration. g) Comparison of different buffers at pH 3, 5, 8, and 10 based on the peak intensity of SO_2 at 625 cm^{-1}. Each data is reported as mean ± SD. h) Heat map of LOD values obtained from the peak intensity of SO_2 at 625 cm^{-1} in three different buffers at pH 3, 5, 8, and 10.

achieved at pH 10. Therefore, it was found that the favored form for our system is sulfite for the interaction with AuNPs within the hydrogel and the highest fraction of the sulfite was reached at pH 10 when compared with pH 8 and pH 5. Moreover, except for pH 3, a good concentration-dependent trend with a good spectral variability was also achieved for pH 5, 8, and 10 in each buffer (Fig. 4d–f).

On the other hand, the best-performing buffer was found as phosphate buffer because it provided not only the highest signal with increased pH but also better discrimination among the different pH values (Fig. 4g). Moreover, when the obtained LOD values were compared, as shown in Fig. 4h, the phosphate buffer provided LOD values down to 0.4 ppm (3.2 μM), while the carbonate buffer provided LOD down to 4.1 ppm (32.8 μM) and the acetate buffer down to 2.1 ppm (16.8 μM). The acetate buffer provided lower intensity values and thus higher LOD because the optimal range of acetate buffer was around 5 and it was forced to pH 8 and 10 with the use of NaOH, which can cause undesired reactions with SO_2, thus reducing the detection efficiency (Vázquez et al., 1988). In the case of carbonate buffer, instead, it is reported that its components can undergo reactions with SO_2 that affect the obtained signals (Keener and Khang, 1993). Thus, the phosphate buffer was selected as the best-performing buffer for further analysis.

2.4. Analytical performance

For the estimation of the LOD (Fig. 5a), signal-to-noise (SNR) values, which are the ratio between the average peak intensity value at 625

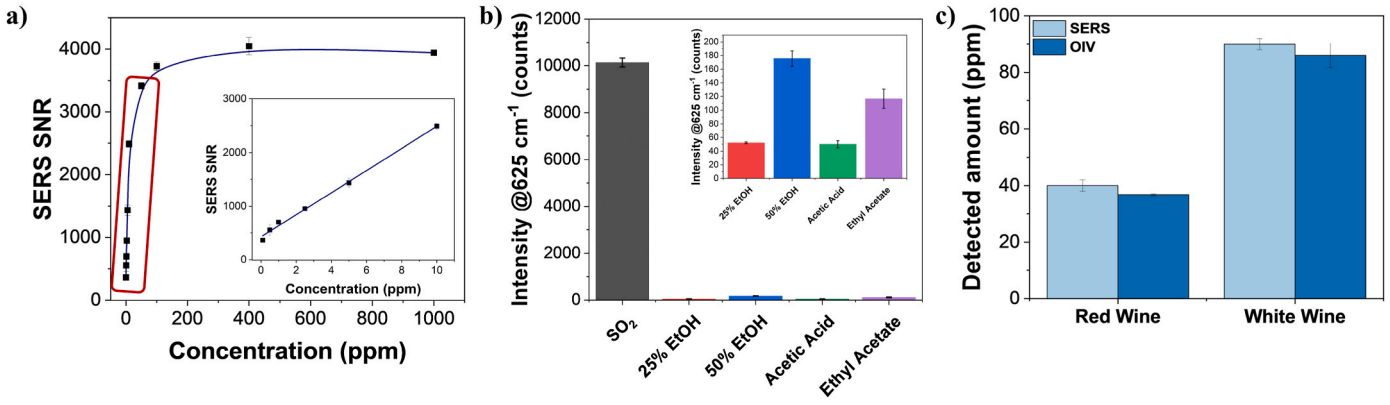

Fig. 5. a) SERS intensity signal-to-noise ratio (SNR) at 625 cm^{-1} as a function of SO_2 concentration (ppm). Inset: Linear range of the curve in the range between 0.1 ppm and 10 ppm. b) Selectivity evaluation of flexible nanocomposites based on the intensity of peak at 625 cm^{-1} with 400 ppm $K_2S_2O_5$, 25% and 50% ethanol (EtOH), 1000 mg L^{-1} acetic acid, and 1000 mg L^{-1} ethyl acetate. Inset: Intensity values in the absence of signal from SO_2. c) Quantification of SO_2 in diluted wine samples by SERS and official OIV-MA-AS323-04B methods.

cm^{-1} and the standard deviation of the spectral region between 2000 and 2100 cm^{-1}, are used. A good dose-response linearity ($R^2 = 0.99$) was achieved in the range of 0.1–10 ppm. Although regular limits are in the range of 150–200 ppm (Stockley et al., 2021) and our real samples have a SO_2 range between 40 and 90 ppm, it should be noted that our real sample measurements are done by diluting wine 10 times with the appropriate buffer (see Section 1.4 of SI). Thus, after dilution of the wine samples, the amount of the SO_2 in wine remains in our linear range. Moreover, LOD was found as 0.4 ppm, which is well below the regular limits for SO_2 in wine as mentioned above.

The selectivity of the proposed device to recognize SO_2 in a complex matrix was assessed by soaking the hydrogel nanocomposites in different solutions containing the different components that are generally found in wine. The peak intensity at 625 cm^{-1} (the peak used for SO_2 detection) was monitored for ethanol, acetic acid, and ethyl acetate (Fig. 5b). At high concentrations of ethanol (25 and 50 % v/v), acetic acid, and ethyl acetate (1000 mg/L for both), no interferences at 625 cm^{-1} were observed as shown also in Fig. S7. As the last step, the performance of the hydrogels was examined on real samples by adjusting the pH of the wine to 10 with dilution in phosphate buffer. In particular, we tested both red and white wines, namely Red Aglianico wine from the 2017 vintage and white Grecomusc' wine from the 2018 vintage (see section 1.9 of SI). The obtained results (Fig. 5c) were compared with the official OIV method and error rates were found as 7.8 and 4.4 %, which showed good consistency between the designed method and the official one.

Consequently, when compared with the state of the art summarized in Table 1, the designed platform is capable of detecting SO_2 down to 0.4 ppm, which is lower than all labeled approaches and competitive with the label-free methods. The power of the designed platform comes from the direct detection of the wine samples with the use of pH dissociation of SO_2 by simply tailoring the pH without any extraction and cleaning steps.

3. Conclusion

SO_2 is one of the most preferred and effective additives used in winemaking due to its antioxidant and antimicrobial properties. Although it can help to maintain many properties of wine such as color, flavor, and freshness, it can cause allergic reactions and thus respiratory and cardiovascular diseases. Due to its possible health risks, the levels of SO_2 required to be monitored. The traditional methods to detect SO_2 in wine are mainly titration-based methods where wine samples are heated and acidified to liberate SO_2 and then analyzed. However, due to the preprocess of samples and the use of headspace sampling methods for detection, existing methods have limited sensitivity and accuracy. Thus, in this study, we proposed the SERS-based pH-dependent detection of SO_2 directly in diluted wine with the use of hydrogel-based nanocomposites based on PEGDA and AuNPs. The all-solution fabrication strategy of hydrogel nanocomposites provided good signal distribution and significant enhancement in the SO_2 signal in dried conditions. The optical properties of AuNPs within the network were proven to be highly stable even after acidic or basic treatments. Furthermore, for the first time, the pH-dependent dissociation of SO_2 was investigated by SERS, and it was found that sulfite is the preferred form for the interaction with AuNPs within the hydrogel. This study showed that pH-dependent dissociation of SO_2 can be used to detect SO_2 directly from liquid samples by simply adjusting the pH of the samples by dilution.

The proposed strategy exhibits high reproducibility and ease of application without the need for complex and costly extraction and sample preparation methods. It eliminated the preprocess of sample and headspace sampling which can cause disruption of SO_2 equilibrium and loss of sample, respectively. Instead of disrupting SO_2 equilibrium, it is used to form the desired form of SO_2 (sulfite) to detect. From liquid samples, the detection of SO_2 down to 0.4 ppm was achieved by just changing the pH of the wine samples to 10. The achieved LOD is approximately three orders of magnitude lower than the legal limits (150–200 ppm in wine). The proposed method can be implemented for any type of wine because, with the use of an appropriate buffer and a simple dilution, pH10 can be obtained regardless of the wine type. At pH10, molecular SO_2 and bisulfite are converted to sulfite form by pH-dependent dissociation of SO_2. Then, the formed sulfite form can be easily detected by the proposed system.

The proposed method provides a low-cost, simple, fast, pre-treatment-free detection of SO_2 in wine directly from its liquid state. Moreover, the total time required for the preparation of the sample and measurements takes less than an hour which shows that the proposed SERS-based detection system can be easily adapted to on-site detection applications with the use of portable spectrometers. It should be also noted that 1500 acquisitions from three independent measurements were acquired to show the reproducibility of the proposed system and it was observed that proposed hydrogel nanocomposites are capable of providing reproducible signals from SO_2. Thus, the required time for the measurement can be lowered up to 5 min while still acquiring 500 acquisitions.

On the other hand, the proposed hydrogel nanocomposite, which can trap small molecules and provide reproducible and high signals, can be implemented to detect other different volatile molecules found in wine during different steps of winemaking including fermentation and aging. The system can be easily adapted to the organic winemaking industry, in which SO_2 levels are much more severely regulated. The use of the device could be easily extended to many different foods and beverages in which SO_2 is used as an additive, such as snacks, fruit juice, fresh or dried vegetables and fruits, jam and marmalade, nuts, seafood, and meat. Finally, this platform could benefit from a portable Raman spectrometer, providing fast and sensitive on-site detection.

CRediT authorship contribution statement

Deniz Yilmaz: Methodology, Validation, Investigation, Data curation, Conceptualization, Writing – original draft, Writing – review & editing. **Bruno Miranda:** Methodology, Validation, Investigation, Software, Data curation, Conceptualization, Writing – original draft, Writing – review & editing. **Enza Lonardo:** Resources, Validation, Writing – review & editing. **Ilaria Rea:** Supervision, Validation, Writing – review & editing. **Luca De Stefano:** Supervision, Conceptualization, Validation, Project administration, Writing – review & editing. **Anna Chiara De Luca:** Supervision, Conceptualization, Validation, Project administration, Writing – review & editing, Funding acquisition.

Declaration of competing interest

The authors declare that they have no known competing financial interests or personal relationships that could have appeared to influence the work reported in this paper.

Data availability

Data will be made available on request.

Acknowledgment

This work was supported by Consiglio Nazionale delle Ricerche, "SEEINVIS" @CNR project (n. SAC.AD002.173.025), and POR CIRO. The authors also thank Giovanna Benvenuto from Stazione Zoologica Anton Dohrn Napoli, Department of Biology and Evolution of Marine Organisms for the help getting SEM images and the Euro-Bioimaging facility. The authors also thank Stefano Managò for helping with preliminary data.

Appendix A. Supplementary data

Supplementary data to this article can be found online at https://doi.org/10.1016/j.bios.2023.115836.

References

Abalde-Cela, S., Auguié, B., Fischlechner, M., Huck, W.T.S., Alvarez-Puebla, R.A., Liz-Marzán, L.M., Abell, C., 2011. Soft Matter 7, 1321–1325.

Aldeanueva-Potel, P., Faoucher, E., Alvarez-Puebla, R.A., Liz-Marzan, L.M., Brust, M., 2009. Anal. Chem. 81, 9233–9238.

Bastús, N.G., Comenge, J., Puntes, V., 2011. Langmuir 27, 11098–11105.

Cavallo, A., Madaghiele, M., Masullo, U., Lionetto, M.G., Sannino, A., 2017. J. Appl. Polym. Sci. 134.

Chen, M., Yang, H., Rong, L., Chen, X., 2016. Analyst 141, 5511–5519.

Coelho, J.M., Howe, P.A., Sacks, G.L., 2015. Am. J. Enol. Vitic. 66, 257–265.

Cojocaru, G.A., Antoce, A.O., 2012. Sci. Pap. Ser. B: Hortic. 56, 457–466.

Corte, L., Roscini, L., Zadra, C., Antonielli, L., Tancini, B., Magini, A., Emiliani, C., Cardinali, G., 2012. Food Chem. 134, 1327–1336.

Deng, Z., Chen, Xuexu, Wang, Y., Fang, E., Zhang, Z., Chen, Xi, 2015. Anal. Chem. 87, 633–640.

Fateixa, S., Daniel-da-Silva, A.L., Nogueira, H.I.S., Trindade, T., 2014. J. Phys. Chem. C 118, 10384–10392.

Gómez-Plaza, E., Bautista-Ortín, A.B., 2019. In: A, M. (Ed.), Emerging Technologies for Aging Wines: Use of Chips and Micro-oxygenation, Red Wine Technology. Academic Press, pp. 149–162.

Grogan, K.A., 2015. Agricultural and Food Economics 3, 19.

Guerrero, R.F., Cantos-Villar, E., 2015. Trends Food Sci. Technol. 42, 27–43.

Howe, P.A., Worobo, R., Sacks, G.L., 2018. Am. J. Enol. Vitic. 69, 210–220.

Huo, N., Li, D., Zheng, S., Deng, W., 2022. Chem. Eng. J. 432, 134317.

Israelsen, N.D., Hanson, C., Vargis, E., 2015. Sci. World J. 124582.

Keener, T., Khang, S.-J., 1993. Chem. Eng. Sci. 48, 2859.

Koch, M., Köppen, R., Siegel, D., Witt, A., Nehls, I., 2010. J. Agric. Food Chem. 58, 9463–9467.

Kong, D., Zhu, W., Li, M., 2021. Microchem. J. 165, 106174.

Lee, W.J., Teschke, K., Kauppinen, T., Andersen, A., J, äppinen, P., Stanczyk Irena, Szadkowska, Pearce, N., Persson, B., Bergeret, A., Facchini, L.A., Kishi, R., Kielkowski, D., Rix, B.A., Henneberger, P., Sunyer, J., Colin, D., Kogevinas, M., Boffetta, P., 2002. Environ. Health Perspect. 110, 991–995.

Li, D., Duan, H., Ma, Y., Deng, W., 2018. Anal. Chem. 90, 5719–5727.

Maier, S.A., 2007. Plasmonics: Fundamentals and Applications. Springer US, New York, NY.

Managò, S., Tramontano, C., Delle Cave, D., Chianese, G., Zito, G., De Stefano, L., Terracciano, M., Lonardo, E., De Luca, A.C., Rea, I., 2021. Small 17, 2101711.

Mandrile, L., Cagnasso, I., Berta, L., Giovannozzi, A.M., Petrozziello, M., Pellegrino, F., Asproudi, A., Durbiano, F., Rossi, A.M., 2020. Food Chem. 326, 127009.

Miranda, B., Rea, I., Dardano, P., De Stefano, L., Forestiere, C., 2021a. Biosensors 11, 107.

Miranda, B., Moretta, R., De Martino, S., Dardano, P., Rea, I., Forestiere, C., De Stefano, L., 2021b. J. Appl. Phys. 129, 033101.

Miranda, B., Moretta, R., Dardano, P., Rea, I., Forestiere, C., De Stefano, L., 2022. Adv. Mater. Technol. 7, 2101425.

Monro, T.M., Moore, R.L., Nguyen, M.-C., Ebendorff-Heidepriem, H., Skouroumounis, G. K., Elsey, G.M., Taylor, D.K., 2012. Sensors 12, 10759–10773.

Nocerino, V., Miranda, B., Tramontano, C., Chianese, G., Dardano, P., Rea, I., De Stefano, L., 2022. Chemosensors 10, 150.

Nuzzo, R.G., Allara, D.L., 1983. J. Am. Chem. Soc. 105, 4481–4483.

Oliveira, S.M., Lopes, T.I., Toth, I.V., Rangel, A.O., 2009. J. Agric. Food Chem. 57, 3415–3422.

Ozbek, N., Akman, S., 2013. J. Agric. Food Chem. 61, 4816–4821.

Paschoalin, R.T., Gomes, N.O., Almeida, G.F., Bilatto, S., Farinas, C.S., Machado, S.A.S., Mattoso, L.H.C., Oliveira, O.N., Raymundo-Pereira, P.A., 2022. Biosens. Bioelectron. 199, 113875.

Pastoriza-Santos, I., Kinnear, C., Pérez-Juste, J., Mulvaney, P., Liz-Marzán, L.M., 2018. Nat. Rev. Mater. 3, 375–391.

Qin, G., Meng, Z., 2009. Food Chem. Toxicol. 47, 734–744.

Ross, C.F., 2012. 2.02 - headspace analysis. In: Pawliszyn, J. (Ed.), Comprehensive Sampling and Sample Preparation. Academic Press, Oxford, pp. 27–50.

Santos, M.C., Nunes, C., Saraiva, J.A., Coimbra, M.A., 2012. Eur. Food Res. Technol. 234, 1–12.

Spaziani, S., Quero, G., Managò, S., Zito, G., Terracciano, D., Macchia, P.E., Galeotti, F., Pisco, M., De Luca, A.C., Cusano, A., 2023. Biosens. Bioelectron. 233, 115322.

Stockley, C., Paschke-Kratzin, A., Teissedre, P.L., Restani, P., Tejedor, N.G., Quini, C., 2021. OIV Collective Expertise Document SO2 and Wine: A Review. OIV Publications, Paris.

Theisen, S., Hänsch, R., Kothe, L., Leist, U., Galensa, R., 2010. Biosens. Bioelectron. 26, 175–181.

Timbo, B., Koehler, K.M., Wolyniak, C., Klontz, K.C., 2004. J. Food Protect. 67, 1806–1811.

Vally, H., Thompson, P., 2001. Thorax 56, 763–769.

Vally, H., Misso, N.L.A., Madan, V., 2009. Clin. Exp. Allergy 39, 1643–1651.

Vázquez, G., Antorrena, G., Chenlo, F., Paleo, F., 1988. Chem. Eng. Technol. 11, 156–162.

Verde, A., Mangini, M., Managò, S., Tramontano, C., Rea, I., Boraschi, D., Italiani, P., De Luca, A.C., 2021. Front. Immunol. 12, 758410.

Xing, T., Qian, Q., Ye, H., Wang, Z., Jin, Y., Zhang, N., Wang, M., Zhou, Y., Gao, X., Wu, L., 2022. Biosens. Bioelectron. 212, 114430.

Xue, Y., Li, X., Li, H., Zhang, W., 2014. Nat. Commun. 5, 4348.